



Cite this: *New J. Chem.*, 2019, 43, 1398

# An L-cysteine-mediated iodide-catalyzed reaction for the detection of I<sup>-</sup>†

Kaili He, Hongyu Chen, Cuiyan Wu,\* Meiling Liu  and Youyu Zhang \*

In this study, a highly selective and eco-friendly fluorescent sensor consisting of upconversion (UCNPs) and gold nanoparticles (AuNPs) was developed for the detection of iodide (I<sup>-</sup>). The negatively charged AuNPs were able to electrostatically adsorb on the positively charged UCNPs, leading to the fluorescence quenching of the UCNPs. In the presence of L-cysteine, AuNPs were released from the surface of the UCNPs and aggregated due to the Au–S interactions that occurred between the AuNPs and L-cysteine, which resulted in the fluorescence recovery of the UCNPs. Upon the addition of I<sup>-</sup>, the fluorescence of the UCNPs was gradually quenched meaning that I<sup>-</sup> catalyzes the oxidation of L-cysteine, preventing the aggregation of AuNPs and forming a fluorescence resonance energy transfer system. The I<sup>-</sup>-catalyzed oxidation reaction provides a method for the L-cysteine-triggered sensor to detect I<sup>-</sup>, using L-cysteine to modulate the fluorescence signal in an eco-friendly manner. Based on the above special detection strategies, this sensor has excellent selectivity for I<sup>-</sup> even in a complex matrix such as urine, which is much better than most assays for I<sup>-</sup>. Under the optimal conditions, the sensor allows the quantitative analysis of I<sup>-</sup> with a detection limit of 55 nM. The high selectivity, sensitivity and environmental friendliness of the sensor proves that it has the potential for the detection of I<sup>-</sup> in actual samples. Most importantly, the excellent results of the sensor for the detection of I<sup>-</sup> in urine prove that the probe can be used as an ideal tool in clinic diagnoses.

Received 29th September 2018,  
Accepted 25th November 2018

DOI: 10.1039/c8nj04944k

rsc.li/njc

## 1. Introduction

Iodine deficiency causes a large range of health problems, including mental retardation, increased perinatal mortality, and hypothyroidism and cretinism, that mainly effect pregnant women and young children.<sup>1</sup> In contrast, excess ingestion of I<sup>-</sup> eventually leads to hyperthyroidism and the formation of a goiter.<sup>2</sup> Therefore, it is crucial to determinate the level of I<sup>-</sup> in order to diagnose and control diseases and disorders that are caused by the dietary deficiency of or abnormal metabolism of I<sup>-</sup>. A large number of countries monitor I<sup>-</sup> status through urinary I<sup>-</sup> levels, which considering that I<sup>-</sup> is mainly excreted by the kidneys, urinary I<sup>-</sup> is a more sensitive indicator to use to detect recent changes in I<sup>-</sup> intake.<sup>1,3</sup> To date, various methods have been reported for the detection of I<sup>-</sup> in urine,<sup>4–8</sup> such as ion-pair reversed-phase HPLC and pulsed amperometric methods<sup>9</sup> that have low quantification limits and high sample throughput, but these are time-consuming procedures. Meanwhile, Ana *et al.* used an electrochemical method to detect I<sup>-</sup> with a low

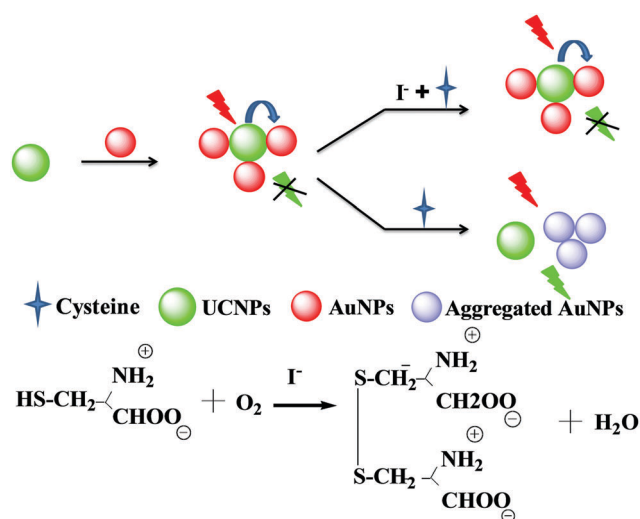
detection limit of  $1.39 \times 10^{-6}$  M.<sup>10</sup> However, this method requires complicated sample preparation processes. Recently, on account of their multifarious advantages such as reliability, high sensitivity and speed, and simple and straightforward operation, fluorescence detection techniques have been regarded as promising and powerful tools for the quantitative detection of I<sup>-</sup>,<sup>11</sup> and fluorogenic chemosensors have been proposed to determine I<sup>-</sup> concentration. However, these fluorescence methods are based on the interaction between I<sup>-</sup> and toxic heavy metal ions, which may influence the selectivity due to their similar chemical properties. For example, He *et al.* prepared carbon dots as a novel probe for the selective determination of I<sup>-</sup>, which exhibited high sensitivity with a low detection limit of 0.234 μM.<sup>12</sup> However, this sensor is based on the strong affinity between I<sup>-</sup> and mercury ions, and mercury ions present a threat to human health and cause serious environmental and health problems. In addition, some of the methods require complicated synthetic procedures.<sup>13</sup> These techniques are rather time-consuming and require tedious chemical modifications and specific operating skills. Hence, it is of the utmost urgency to develop a facile, low-cost, and environmentally friendly method for the detection of I<sup>-</sup>.

Fluorescence resonance energy transfer (FRET) has sparked great attention in the field of detection systems due to its unique advantages, including accuracy, precision, and high sensitivity. The two major components in FRET are energy

*Key Laboratory of Chemical Biology and Traditional Chinese Medicine Research (Ministry of Education), College of Chemistry and Chemical Engineering, Hunan Normal University, Changsha 410081, P. R. China. E-mail: zhangyy@hunnu.edu.cn, cuiyan.wu@hunnu.edu.cn; Fax: +86-731-88865515; Tel: +86-731-88865515*

† Electronic supplementary information (ESI) available. See DOI: 10.1039/c8nj04944k

donors and acceptors. Among the many materials used in FRET-based analysis, upconversion nanoparticles (UCNPs), as a class of materials, have been verified to be efficient and promising energy donors. Rare-earth (RE) doped UCNPs, which convert low-energy near-infrared (NIR) light into a higher-energy output photon with a shorter wavelength *via* a two-photon or multiphoton mechanism, have attracted wide attention.<sup>14</sup> UCNPs have been extensively applied in *in vivo* fluorescence imaging and the real-time monitoring of drug delivery,<sup>15–17</sup> on account of their low toxicity, narrow emission peaks and high photostability, greater tissue penetration, and minimal photo-damage to organisms.<sup>18</sup> In comparison with traditional semiconductor quantum dots and organic fluorophores,<sup>19</sup> UCNPs are capable of increasing the sensitivity because there is no autofluorescence interference from biomolecules.<sup>20</sup> Therefore, UCNPs have been extensively applied in biosensing.<sup>21–23</sup> In this work, an off-on-off fluorescence probe for I<sup>−</sup> sensing based on the I<sup>−</sup>-catalyzed oxidation of cysteine to cystine, has been designed and developed and a schematic of this process is shown in Scheme 1. In this nanosystem, many negatively charged AuNPs conjugate with positively charged UCNPs through electrostatic interactions, resulting in the fluorescence quenching of UCNPs (turn-off). The presence of Au–S bonds between the L-cysteine and AuNPs led to the aggregation of the AuNPs, and the simultaneous release of the AuNPs from the surface of the UCNPs induced the UCNP fluorescence recovery (turn-on). In contrast, since I<sup>−</sup> can catalyze the oxidation of thiol compounds by dissolving oxygen to form disulfide compounds,<sup>24</sup> and the disulfide and the L-cystine did not cause the aggregation of the AuNPs and formed an energy transfer system between the UCNPs and AuNPs, the fluorescence recovered by L-cysteine was effectively quenched (turn-off). More importantly, this work creates an eco-friendly system that uses L-cysteine rather than mercury ions or other toxic heavy metal ions to modulate the fluorescence signals to detect I<sup>−</sup> in urine samples.



**Scheme 1** Schematic illustration of the mechanism of I<sup>−</sup> detection using the UCNP and AuNP probe.

## 2. Experimental

### 2.1. Materials and apparatus

Lanthanide oxides (Y<sub>2</sub>O<sub>3</sub>, Yb<sub>2</sub>O<sub>3</sub>, Er<sub>2</sub>O<sub>3</sub>) were obtained from the China National Pharmaceutical Group Corporation (Shanghai, China). All of the rare earth lanthanide oxides were 99.9% purity or higher. The lanthanide oxides were dissolved in hot nitric acid and then diluted with deionized water to achieve final concentrations of 0.4 M. Chloroauric acid (HAuCl<sub>4</sub>) and hexadecyl trimethyl ammonium bromide (CTAB) were obtained from Sigma (Shanghai, China), L-cysteine, Na<sub>2</sub>C<sub>2</sub>O<sub>4</sub>, Na<sub>2</sub>SO<sub>4</sub>, NaF, NaCl, NaBr, Na<sub>2</sub>HPO<sub>4</sub>, NaNO<sub>3</sub>, NaIO<sub>3</sub>, NaClO<sub>3</sub>, citrate, CH<sub>3</sub>COONa, NaH<sub>2</sub>PO<sub>4</sub>, NaClO<sub>4</sub>, NaNO<sub>2</sub>, Na<sub>2</sub>SiO<sub>3</sub>, and KI were purchased from Beijing Chemical Corp. All other chemicals (99%, Merck) used in this work were of analytical grade and Millipore Milli-Q ultrapure water was used throughout the experiments. A UV-2450 spectrophotometer (Shimadzu Co., Japan) was used to record the UV-vis absorption spectra. The fluorescence spectra were measured by an F-4500 fluorescence spectrophotometer (Hitachi Ltd, Japan) with an external 980 nm laser diode (Hi-Tech Optoelectronic Co., Ltd China) as the excitation source. Transmission electron microscopy (TEM) images were collected by a JEOL-1230 transmission electron microscope (JEM-3010 Jeol, Japan). The ζ potential measurements were performed by a Nano-ZS Zetasizer ZEN3600 (Malvern Instruments Ltd, UK). FT-IR spectra of samples were obtained using an FT-IR spectrometer (Nicolet Instrument Co., USA).

### 2.2. Synthesis of the UCNPs

The NaYF<sub>4</sub>:Yb<sup>3+</sup>,Er<sup>3+</sup> UCNPs were synthesized according to previously reported methods.<sup>25,26</sup> Firstly, 7.5 mL of 0.1 M sodium trisodium citrate was added to a solution mixture containing 8.8 mL of 0.1 M Y(NO<sub>3</sub>)<sub>3</sub>, 1.0 mL of 0.1 M Yb(NO<sub>3</sub>)<sub>3</sub> and 0.2 mL of 0.1 M Er(NO<sub>3</sub>)<sub>3</sub> under stirring, then 25 mL of ethanol and 0.2 g of cetyl trimethylammonium bromide (CTAB) were added to the above solution under stirring for 15 min at room temperature. 12 mL of 0.1 M NaF was added dropwise to the homogeneous solution under continuous stirring over 1 h until the solution became clear. Next, 2 mL of HNO<sub>3</sub> was added into the precursor solution and the solution mixture was transferred to a 100 mL Teflon-lined autoclave and then sealed and heated at 180 °C for 4 h. Finally, the reaction solution was cooled down to room temperature and the nanocrystals were collected by centrifugation at 10 000 rpm. The product was cleaned by washing four times with ethanol and Milli-Q ultrapure water in sequence and the precipitate was dried in an oven at 98 °C.

### 2.3. Synthesis of the AuNPs

AuNPs were synthesized by the citrate reduction of HAuCl<sub>4</sub> according to the method described in the previous literature.<sup>27,28</sup> In general, an aqueous solution (including 0.5 mL of 2% HAuCl<sub>4</sub>) of 100 mL of HAuCl<sub>4</sub> was heated to 100 °C, then 1.8 mL of a 1% sodium citrate solution was quickly mixed into the boiling HAuCl<sub>4</sub> solution under vigorous magnetic stirring. The mixed solution

was boiled for 10 min, further followed by constant stirring without heating for another 15 min. The nearly colorless original solution turned pale yellow and finally wine-red, typical phenomena observed during the preparation of AuNPs, and then a stable AuNP solution was obtained.

#### 2.4. Experimental procedure for the fluorescence detection of I<sup>-</sup>

Various amounts of different concentrations of I<sup>-</sup> were incubated with L-cysteine (12 μM) solution, then UCNPs (0.01 mg mL<sup>-1</sup>), AuNPs (1.25 nM) and PBS (10 mM, pH = 8.0) were added into each mixture (the final volume is 500 μL). The mixtures were incubated for 45 min at 45 °C and then fluorescence emission spectra were measured with an excitation wavelength of 980 nm.

### 3. Results and discussion

#### 3.1. Characteristics of the UCNPs and AuNPs

The morphology, crystallographic phase, distribution of the surface groups, as well as the optical properties of the UCNPs have been characterized. The TEM image shown in Fig. 1A shows that the synthesized UCNPs possess a globular shape distribution, with an average size of around 30 nm in diameter. As presented in Fig. S1A (ESI<sup>†</sup>), the XRD pattern showed no difference between the prepared UCNPs and the standard values for JCPDS no. 77-2042, indicating that the UCNPs were successfully synthesized in high crystallinity. The FT-IR spectrum of the UCNPs (curve 2 in Fig. S1B, ESI<sup>†</sup>) was identical to that of pure CTAB (curve 1 in Fig. S1B, ESI<sup>†</sup>). As shown in Fig. S1B (ESI<sup>†</sup>) (curve 2), the UCNPs possessed broad absorption bands at 2986 cm<sup>-1</sup> and 2831 cm<sup>-1</sup> that can be attributed to C-H (-CH<sub>3</sub> and -CH<sub>2</sub>-) stretching and had a weak absorption near 1597 cm<sup>-1</sup> due to the absorptions in the region characteristic of amine groups (-NH<sub>2</sub>). The FT-IR spectrum demonstrated that CTAB partly covered the surface of the UCNPs. After amino modification of the UCNPs, the UCNPs exhibited excellent stability and dispersibility in water and the fluorescence intensity remained unchanged within 60 min (Fig. S2A, ESI<sup>†</sup>). As shown in Fig. S2B (ESI<sup>†</sup>), different pH values have little influence on the fluorescence intensity of the UCNPs. The fluorescence spectroscopy of the UCNPs collected in aqueous solution revealed two characteristic peaks at 554 and 667 nm under 980 nm laser excitation, which can be assigned to

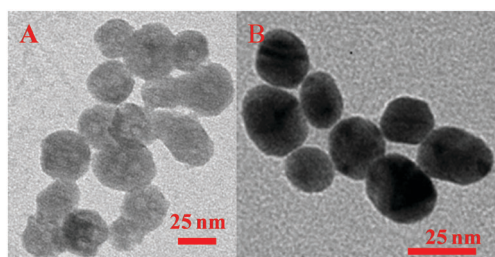


Fig. 1 TEM images of the UCNPs (A) and AuNPs (B).

transitions from the <sup>4</sup>S<sub>3/2</sub>, and <sup>4</sup>F<sub>9/2</sub> excited states to the <sup>4</sup>I<sub>15/2</sub> ground state, respectively.<sup>29</sup>

The morphology and absorption spectrum of the AuNPs were investigated using TEM and UV-vis spectroscopy. As is vividly shown in the Fig. 1B, the AuNPs show a spherical structure with a size of approximately 25 nm in diameter. In addition, the AuNPs have a characteristic surface plasmon resonance (SPR) peak located at 524 nm when characterized by UV-vis spectroscopy.

#### 3.2. Fluorescence resonance energy transfer (FRET) between the UCNPs and AuNPs

To verify the FRET between the UCNPs and AuNPs, the ζ-potentials were determined. As presented in Fig. S3 (ESI<sup>†</sup>), the ζ-potentials values of the dispersed UCNPs and AuNPs in PBS buffer were measured as +38.3 mV and -31.3 mV, respectively. These values manifest that the UCNP nanospheres are positively charged, in contrast, the AuNPs are negatively charged in solutions, which suggests that the UCNPs were conjugated with AuNPs through electrostatic attractions. In addition, the UV-vis absorption and fluorescence emission spectra were also recorded. As shown in Fig. 2, curve b shows the characteristic peaks of the AuNPs at 524 nm, and the main emission peak of the UCNPs appeared in 550 nm, with the absorption spectrum of the AuNPs largely overlapping the emission spectrum of the UCNPs. Considering the above two aspects, we speculate that the fluorescence quenched mechanism of the AuNPs to the UCNPs was based on FRET.<sup>30</sup> As shown in Fig. S4A (ESI<sup>†</sup>), the effect of the concentration of the AuNPs on the fluorescence quenching efficiency was studied in detail. Through analysis, we can conclude that the fluorescence intensity of the UCNPs gradually decreased upon an increase in the AuNP concentration. The Stern-Volmer equation was applied to calculate the quenching constant:<sup>31</sup>

$$I_0/I = K_{sv} \times [Q] + 1$$

*I* and *I*<sub>0</sub> represent the fluorescence intensity in the absence and presence of the AuNPs, respectively. The concentration of the

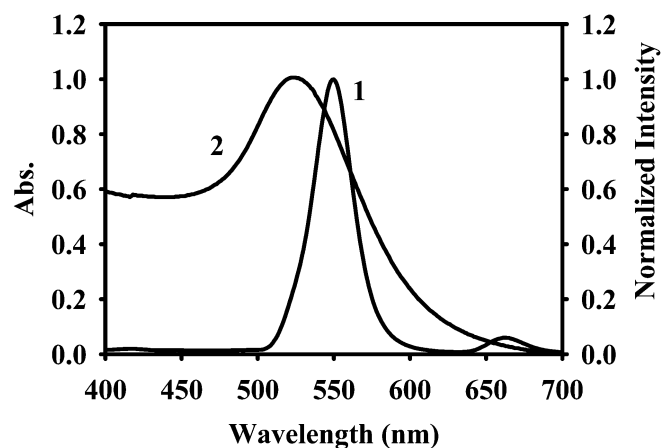


Fig. 2 Emission spectrum of the UCNPs (1) and absorption spectrum of the AuNPs (2).

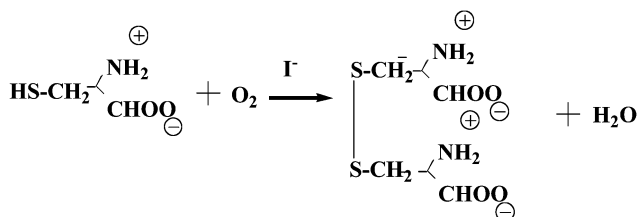
AuNPs is represented by Q. As described in Fig. S4B (ESI<sup>†</sup>), the linear relationship between  $I_0/I$  and the concentration of the AuNPs can be written in a rearranged form of the well-known Stern–Volmer equation:

$$I_0/I = 1.928 \times [Q] + 1 \quad (R^2 = 0.9950)$$

The quenching constant ( $K_{sv}$ ) was found to be  $1.928 \times 10^9$ , which was calculated using the Stern–Volmer equation. According to the quenching constant, the AuNPs were found to remarkably quench the fluorescence of the UCNPs.

### 3.3. The strategy of $I^-$ detection

The detection mechanism is primarily based on the following reactions:<sup>24</sup>



Based on the above reactions, it is believed that  $I^-$  acted as a catalyst in the transformation of L-cysteine to L-cystine, which caused the dispersion of the AuNPs. As can be seen from Fig. 3, the fluorescence intensity of the as-prepared UCNP solution was significantly enhanced centered at around 550 nm (curve 1), and the sensitivities were increased in that the UCNPs resulted in an enhanced signal-to-background ratio. The introduction of the AuNPs induced a decrease in the fluorescence intensity of the UCNPs due to the occurrence of the FRET process (curve 2). After adding L-cysteine into the UCNP and AuNP solution mixture, the L-cysteine caused the aggregation of the AuNPs, which broke the FRET system and thus resulted in the recovery of the fluorescence intensity of the UCNPs (curve 3). On the contrary, after  $I^-$  was incubated with L-cysteine,

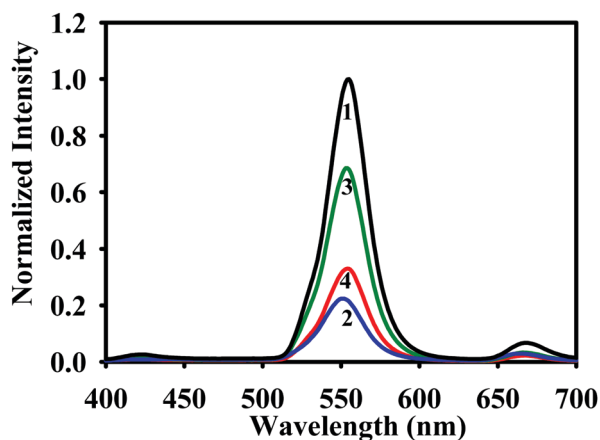


Fig. 3 Normalized fluorescence intensity of the UCNPs (1), UCNPs and AuNPs (2), the of UCNP–AuNP–L-cysteine solution mixture (3), and the UCNPs and AuNPs after adding L-cysteine and  $I^-$  (4). [UCNPs]:  $0.1 \text{ mg mL}^{-1}$ ; [AuNPs]:  $1.25 \text{ nM}$ ; [L-cysteine]:  $12 \text{ }\mu\text{M}$ ; [ $I^-$ ]:  $200 \text{ }\mu\text{M}$ ; PBS:  $0.01 \text{ M}$ .

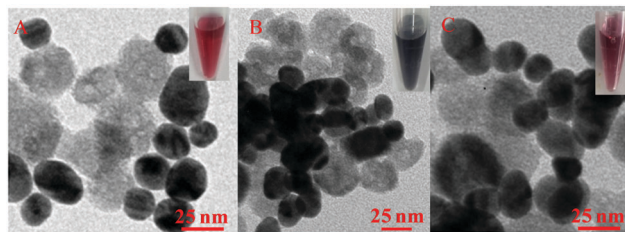


Fig. 4 TEM images of the UCNPs in the presence of the AuNPs (A), UCNPs–AuNPs after adding L-cysteine (B) and UCNPs–AuNPs upon pretreating L-cysteine with  $I^-$  (C). [UCNPs]:  $0.1 \text{ mg mL}^{-1}$ ; [AuNPs]:  $1.25 \text{ nM}$ ; [L-cysteine]:  $12 \text{ }\mu\text{M}$ ; [ $I^-$ ]:  $200 \text{ }\mu\text{M}$ ; PBS:  $0.01 \text{ M}$ .

$I^-$  catalyzed the oxidation of thiol compounds to form disulfide compounds<sup>18</sup> that prevented the aggregation of AuNPs and thus resulted in a decrease in the fluorescence intensity of the UCNPs (curve 4). The interaction between  $I^-$ , L-cysteine, the UCNPs and the AuNPs was further evidenced from TEM images. As shown in Fig. 4A, in the presence of the UCNPs, the AuNPs remained in a dispersed state and the solution mixture maintained its red color. When L-cysteine was added into the UCNPs–AuNPs solution mixture, as shown in Fig. 4B, the color of the solution became blue and the AuNPs aggregated due to the Au–S bonds between L-cysteine and the AuNPs. In contrast, when both of L-cysteine and  $I^-$  were present, the solution was red in color (Fig. 4C) and the AuNPs remained dispersed in that  $I^-$  acts as a catalyst in the oxidation of L-cysteine to yield L-cystine, which prevents the aggregation of the AuNPs. In addition, the  $I^-$  catalyzed oxidation of the thiol compounds was verified from FT-IR spectra, as shown in Fig. S5 (ESI<sup>†</sup>). For L-cysteine, the peak of the stretching vibration of  $-\text{SH}$  was located at  $2556 \text{ cm}^{-1}$ . After the treatment of the  $I^-$  solution, the peak at  $2556 \text{ cm}^{-1}$  disappeared, indicating that the oxidation of  $-\text{SH}$  was successfully catalyzed by  $I^-$ . Consequently, all of these results successfully explain the sensing principle of the detection of  $I^-$ .

### 3.4. Optimization of the detection conditions

To obtain high detection sensitivity and achieve better analytical performances for the detection of  $I^-$ , factors such as pH, L-cysteine concentration, incubation time, and reaction temperature were investigated. A large amount of L-cysteine was found to assemble on the surface of the AuNPs, which prevented the FRET process between the UCNPs and AuNPs and thus allowed the recovery of the fluorescence intensity of the UCNPs. As shown in Fig. 5A, the fluorescence recovery was observed to have no obvious differences when the concentration of L-cysteine was more than  $12 \text{ }\mu\text{M}$ . Moreover, a higher concentration would be less efficient and unfavorable for lowering the detection limit. Therefore, a concentration of L-cysteine of  $12 \text{ }\mu\text{M}$  was employed for the following studies. In order to realize a complete reaction, the incubation time was explored. Fig. 5B shows that the fluorescence intensity decreased along upon an increase in the reaction time from 0 to 40 min, and remained constant after 40 min, illustrating that the  $I^-$ -catalyzed oxidation of L-cysteine to L-cystine could be sufficiently completed within 40 min. Thus, the optimal

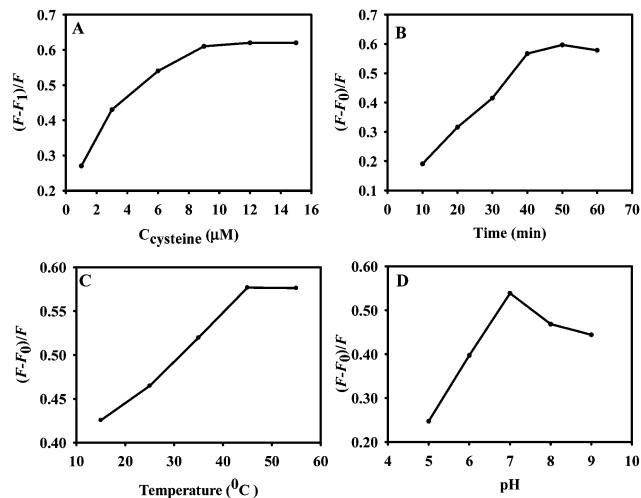


Fig. 5 Effects of L-cysteine concentration (A), and incubation time (B), incubation temperature (C) and pH (D) on the fluorescent sensor for I<sup>-</sup> detection.

reaction time was determined as 40 min. The temperature effects are summarized in Fig. 5C. The I<sup>-</sup>-catalyzed oxidation of L-cysteine to L-cystine at different temperatures shows that the increase in the temperature accelerated the reaction process. The fluorescence of the nanoprobe hardly changed when the temperature was greater than 45 °C, indicating that the nanoprobe is stable under 45 °C. The pH value of the solution had a great influence on the rate of the oxidation of I<sup>-</sup>, which was investigated in our work. As shown in Fig. 5D, the fluorescence quenching reached a maximum at pH 7, so it can be concluded that at the pH value obtained in this experiment that L-cysteine was rapidly oxidized to L-cystine by oxygen in solution.

### 3.5. Performance of the sensor

Under the optimal conditions, solutions with different concentrations of I<sup>-</sup> were detected using the abovementioned fluorescence method. Fig. 6A manifest that a series of different concentrations of I<sup>-</sup> contributed to different levels of fluorescence quenching of the UCNPs in the PBS buffer solution. As discussed above,  $(F - F_0)/F$  was chosen as the output signal, in which  $F_0$  and  $F$  refer to the fluorescence intensities of the UCNP–AuNP–L-cysteine–I<sup>-</sup> solution mixtures in the presence of different concentrations of and absence of I<sup>-</sup>, respectively.  $F_1$  refers to the fluorescence intensity of the UCNPs–AuNPs at 550 nm in the absence of L-cysteine and I<sup>-</sup>, and its variation is shown in Fig. 6B. There was a significant inverse correlation between  $(F - F_0)/F$  and the concentrations of I<sup>-</sup> from 0.1 to 200 μM, as expressed by the linear regression equation  $(F - F_0)/F = 0.2235 + 0.1586 \log[I^-] (\mu\text{M})$  ( $R^2 = 0.9887$ ). The limit of detection (LOD) for I<sup>-</sup> calculated using the  $3\sigma/s$  criteria was 55 nM, which represents a high enough sensitivity for the detection of I<sup>-</sup>. In the summary and contrastive analysis, a comparison between the developed sensors and other reported methods for I<sup>-</sup> detection was obtained, as presented in Table S1 (ESI<sup>†</sup>), and it was confirmed that the developed sensors could achieve a more sensitive detection than other reported methods.

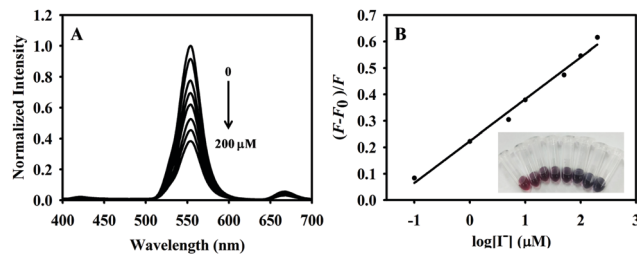


Fig. 6 (A) The overlaid fluorescence spectra of the UCNP–AuNP–L-cysteine solution with various concentrations of I<sup>-</sup>. The concentrations of I<sup>-</sup> (from top to bottom) are 0.1 μM, 1 μM, 5 μM, 10 μM, 50 μM, 100 μM, and 200 μM, respectively. [UCNPs]: 0.1 mg mL<sup>-1</sup>; [AuNPs]: 1.25 nM; [L-cysteine]: 12 μM; PBS: 0.01 M, and (B) the linear relationship between the quenching efficiency  $(F - F_0)/F$  and I<sup>-</sup> concentrations from 0.1 to 200 μM.

Selectivity and specificity are important factors in developing an excellent sensor. In this work, the optical UCNP–AuNP–L-cysteine–I<sup>-</sup> mixed nanosystem was extended to the detection of other ions. I<sup>-</sup> with a final concentration of 200 μM was used to evaluate the selectivity towards various metal ions (including C<sub>2</sub>O<sub>4</sub><sup>2-</sup>, SO<sub>4</sub><sup>2-</sup>, F<sup>-</sup>, Cl<sup>-</sup>, Br<sup>-</sup>, HPO<sub>4</sub><sup>2-</sup>, NO<sub>3</sub><sup>-</sup>, IO<sub>3</sub><sup>-</sup>, ClO<sub>3</sub><sup>-</sup>, citrate, CH<sub>3</sub>COO<sup>-</sup>, H<sub>2</sub>PO<sub>4</sub><sup>-</sup>, ClO<sub>4</sub><sup>-</sup>, NO<sub>2</sub><sup>-</sup>, and SiO<sub>3</sub><sup>2-</sup>). Different metal ions were added into the UCNP, AuNP, and L-cysteine solution with a final concentration of 2 mM, then the fluorescence spectra were recorded under excitation at 980 nm to study the selectivity. Fig. 7 shows that the fluorescence intensity decreased remarkably upon the addition of I<sup>-</sup>, whereas other ions had negligible or less impact on the intensity. This indicates that the UCNP–AuNP–L-cysteine–I<sup>-</sup> system has high selectivity towards I<sup>-</sup>.

### 3.6. Application in real samples

Human urine samples were collected from the Hospital of Hunan Normal University (Changsha, China). The study complied with all institutional and national guidelines, as per the Institutional Ethics Committee. The protocol was approved by the College of Chemistry and Chemical Engineering,

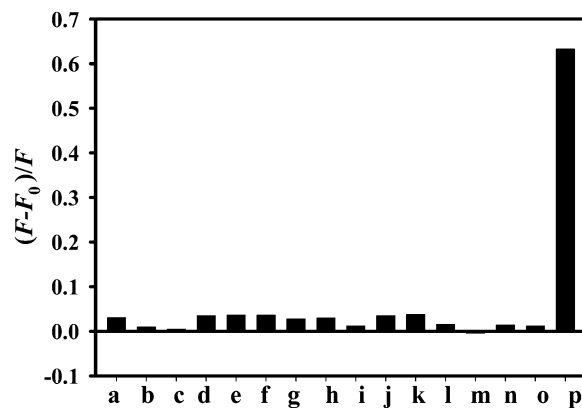


Fig. 7 Fluorescence spectra of the UCNP–AuNP–L-cysteine nanosensor in the presence of 200 μM I<sup>-</sup> or 2 mM other anions. [UCNPs]: 0.1 mg mL<sup>-1</sup>; [AuNPs]: 1.25 nM; [L-cysteine]: 12 μM; PBS: 0.01 M (a) C<sub>2</sub>O<sub>4</sub><sup>2-</sup>, (b) SO<sub>4</sub><sup>2-</sup>, (c) F<sup>-</sup>, (d) Cl<sup>-</sup>, (e) Br<sup>-</sup>, (f) HPO<sub>4</sub><sup>2-</sup>, (g) NO<sub>3</sub><sup>-</sup>, (h) IO<sub>3</sub><sup>-</sup>, (i) ClO<sub>3</sub><sup>-</sup>, (j) citrate, (k) CH<sub>3</sub>COO<sup>-</sup>, (l) H<sub>2</sub>PO<sub>4</sub><sup>-</sup>, (m) ClO<sub>4</sub><sup>-</sup>, (n) NO<sub>2</sub><sup>-</sup>, (o) SiO<sub>3</sub><sup>2-</sup>, and (p) I<sup>-</sup>, respectively.

Table 1 Detection of I<sup>-</sup> in urine samples

Urine sample	Spiked (μM)	Measured (μM)	Recovery (%)	RSD (n = 3, %)
1	0.1	0.11	110.0	4.86
2	10	9.82	98.20	1.67
3	100	95.83	95.83	1.90

Hunan Normal University. The person donating the human urine gave informed written consent.

On further demonstrating the feasibility and repeatability of the UCNPs–AuNPs probe for practical applications, urine samples, spiked with different concentrations of I<sup>-</sup>, were used as real samples. Insoluble substances in the urine samples were removed by centrifugation (1000 rpm, 20 min) and filtration through a 0.2 μm membrane, then the filtered urine was diluted 50 times with a PBS buffer solution. The recovery experiments were performed using urine samples as a matrix to verify the method. The recoveries of I<sup>-</sup> are exhibited in Table 1, ranging from 95.83% to 110.00% for the real samples, with relative standard deviation (RSD, n = 3) values in the range of 1.67% to 4.86%, indicating the prospect of using the developed system.

## 4. Conclusions

In summary, a simple and off–on–off fluorescence probe for the detection of I<sup>-</sup> was developed. For this purpose, we used L-cysteine to modulate the fluorescence signals of the UCNPs for I<sup>-</sup> detection. By combining the highly selective I<sup>-</sup>-catalyzed oxidation reaction with the nonautofluorescence benefits of the UCNPs, a sensitive, eco-friendly and highly selective sensing approach for I<sup>-</sup> detection was designed and applied to monitor I<sup>-</sup> levels in human urine. It is believed that this strategy will provide a new approach for developing highly sensitive and selective sensors for use in environmental and biological sensing applications.

## Conflicts of interest

There are no conflicts to declare.

## Acknowledgements

This work was supported by the National Natural Science Foundation of China (21874042 and 21675051), and the Foundation of the Science & Technology Department of Hunan Province (2016SK2020).

## Notes and references

- 1 B. De Benoist, M. Andersson, I. M. Egli and T. El Bahi, H. Allen and W. H. Organization, *Iodine status worldwide*, 2004.
- 2 F. Azizi, M. Hedayati, M. Rahmani, R. Sheikholeslam, S. Allahverdian and N. Salarkia, *J. Endocrinol. Invest.*, 2005, **28**, 23–29.

- 3 M. B. Zimmermann, *Semin. Cell Dev. Biol.*, 2011, **22**, 645.
- 4 Q. Lin, T. T. Lu, X. Zhu, T. B. Wei, H. Li and Y. M. Zhang, *Chem. Sci.*, 2016, **7**, 5341–5346.
- 5 Z. Zhang, Z. Chen, F. Cheng, Y. Zhang and L. Chen, *Analyst*, 2016, **141**, 2955–2961.
- 6 L. Chen, W. Lu, X. Wang and L. Chen, *Sens. Actuators, B*, 2013, **182**, 482–488.
- 7 H. Huang, Y. Weng, L. Zheng, B. Yao, W. Weng and X. Lin, *J. Colloid Interface Sci.*, 2017, **506**, 373–378.
- 8 Q. Lin, P. P. Mao, Y. Q. Fan, L. Liu, J. Liu, Y. M. Zhang, H. Yao and T. B. Wei, *Soft Matter*, 2017, **13**, 7085–7089.
- 9 V. T. Nguyen, V. Piersoel and M. T. El, *Talanta*, 2012, **99**, 532–537.
- 10 A. Machado, R. B. Mesquita, S. Oliveira and A. A. Bordalo, *Talanta*, 2017, **167**, 688.
- 11 L. Zhu, X. Peng, H. Li, Y. Zhang and S. Yao, *Sens. Actuators, B*, 2017, **238**, 196–203.
- 12 J. He, H. Zhang, J. Zou, Y. Liu, J. Zhuang, Y. Xiao and B. Lei, *Biosens. Bioelectron.*, 2015, **79**, 531.
- 13 S. C. Wei, P. H. Hsu, Y. F. Lee, Y. W. Lin and C. C. Huang, *ACS Appl. Mater. Interfaces*, 2012, **4**, 2652–2658.
- 14 S. Wu, N. Duan, Z. Shi, C. Fang and Z. Wang, *Anal. Chem.*, 2014, **86**, 3100.
- 15 Y. Feng, H. Chen, L. Ma, B. Shao, S. Zhao, Z. Wang and H. You, *ACS Appl. Mater. Interfaces*, 2017, **9**, 15096–15102.
- 16 M. Lin, Y. Gao, T. J. Diefenbach, J. K. Shen, F. J. Hornicek, Y. I. Park, F. Xu, T. J. Lu, M. Amiji and Z. Duan, *ACS Appl. Mater. Interfaces*, 2017, **9**, 7941.
- 17 J. Lai, B. P. Shah, Y. Zhang, L. Yang and K. B. Lee, *ACS Nano*, 2015, **9**, 5234–5245.
- 18 K. Zhu, G. Liu, J. Hu and S. Liu, *Biomacromolecules*, 2017, **18**, 2571.
- 19 J. Li, X. Hong, D. Li, K. Zhao, L. Wang, H. Wang, Z. Du, J. Li, Y. Bai and T. Li, *Chem. Commun.*, 2004, 1740–1741.
- 20 H. Du, J. Yu, D. Guo, W. Yang, J. Wang and B. Zhang, *Langmuir*, 2016, **32**, 1155.
- 21 Q. Long, H. Li, Y. Zhang and S. Yao, *Biosens. Bioelectron.*, 2015, **68**, 168–174.
- 22 H. Chen, A. Fang, Y. Zhang and S. Yao, *Talanta*, 2017, **174**, 148.
- 23 Q. Wu, L. Qian, H. Li, Y. Zhang and S. Yao, *Talanta*, 2015, **136**, 47–53.
- 24 Y. Xianyu, Y. Chen and X. Jiang, *Anal. Chem.*, 2015, **87**, 10688.
- 25 H. Q. Chen, F. Yuan and L. Wang, *Anal. Methods*, 2013, **5**, 2873–2879.
- 26 J. Chen, H. Chen, C. Zhou, J. Xu, F. Yuan and L. Wang, *Anal. Chim. Acta*, 2012, **713**, 111.
- 27 G. Sener, L. Uzun and A. Denizli, *Anal. Chem.*, 2014, **86**, 514–520.
- 28 J. Hu, Z. Wang and J. Li, *Sensors*, 2007, **7**, 3299–3311.
- 29 B. Yin, W. Zhou, Q. Long, C. Li, Y. Zhang and S. Yao, *CrystEngComm*, 2014, **16**, 8348–8355.
- 30 L. Wang, R. Yan, Z. Huo, L. Wang, J. Zeng, J. Bao, X. Wang, Q. Peng and Y. Li, *Angew. Chem., Int. Ed. Engl.*, 2005, **44**, 6054–6057.
- 31 J. Zhao, Y. Yi, N. Mi, B. Yin, M. Wei, Q. Chen, H. Li, Y. Zhang and S. Yao, *Talanta*, 2013, **116**, 951–957.